Science Advances
AAAS

Manuscript Template

FRONT MATTER

Excited State Intramolecular Proton Transfer in Hydroxyanthraquinones: Towards Predicting Fading of Organic Red Colorants in Art

Authors
J.A. Berenbeim,[1] S. Boldissar,[1§] S. Owens,[1] M.R. Haggmark,[1] G. Gate,[1] F.M. Siouri,[1] T. Cohen,[1] M. F. Rode,[2] C. Schmidt Patterson,[3] and M.S. de Vries[1]*

Affiliations
[1] Department of Chemistry and Biochemistry, University of California Santa Barbara, California, USA.
[2] Institute of Physics, Polish Academy of Sciences, Al. Lotnikow 32/46 02-668, Warszawa Poland.
[3] Getty Conservation Institute, 1200 Getty Center Drive, Suite 700, Los Angeles, California, USA.
* E-mail: devries@chem.ucsb.edu

Abstract

Compositionally similar organic red colorants in the anthraquinone family, whose photodegradation can cause irreversible color and stability changes, have long been used in works of art. Different organic reds, and their multiple chromophores, suffer degradation disparately. Understanding the details of these molecules' degradation, therefore, provides a window into their behavior in works of art, and may assist the development of improved conservation methods. According to one proposed model of photodegradation dynamics, intramolecular proton transfer provides a kinetically favored decay pathway in some photo-excited chromophores, preventing degradation-promoting electron transfer (ET). To further test this model, we measured excited state lifetimes of substituted gas phase anthraquinones, utilizing high-level theory to explain the experimental results. The data show a general structural trend: anthraquinones with 1,4-OH substitution are long-lived and prone to damaging ET, while excited state intramolecular proton transfers promote efficient quenching for hydroxyanthraquinones that lack this motif.

Introduction

Exposure to light degrades many molecules when absorption of ultraviolet and visible wavelength photons places them in an energetically excited state prone to chemical and physical change. Molecules susceptible to photodegradation are ubiquitous in both natural and synthetic systems and undesired effects of such degradation can include a wide range of phenomena, such as the

§ Samuel Boldissar tragically passed away following a rock climbing accident.

appearance of abnormal skin cells marking melanoma, and the drop of efficiency in polymer solar cells via photo-bleaching. One notable form of organic photodegradation with relevance to the broad field of cultural heritage research is the fading of certain chromophores in works of art, which leads to visual change in a medium where meaning and value is often predicated on color.

Natural organic red colorants of either plant or scale-insect origin are important traditional sources of red hues.(*1*) These colorants have high tinting strength and are therefore present on artifacts in low concentration; as little as subnanogram concentrations of these colorants may be required to achieve a desired color saturation.(*2*) Many traditional organic red colorants (including madder, alizarin, cochineal, lac dye, brazilwood, and dragonsblood) are compositionally similar: these anthraquinones (AQ) and hydroxyanthraquinones (HAQ) have long been used as lake pigments and contain primarily hydroxyl, carboxylic acid, and carbonyl moieties on a conjugated aromatic backbone. While commercial interest in AQs and HAQs has recently expanded to include pharmaceutical applications,(*3, 4*) the use of natural AQ derivatives (see Fig. 1) as lake dyes (insoluble dye-mordant complexes, typically precipitated with Al or Ca cations) has long attracted the attention of fine artists and craftsmen, and these pigments continue to be used today. The irreversible fading of organic red colorants in art is well-documented, and greatly affects the perception of masterpieces from antiquity to the present day. Recent publications, for example, have highlighted alteration of organic red colorants in objects as disparate as medieval manuscript illuminations to paintings by Vincent van Gogh.(*5-7*)

One of the simplest HAQ molecules to be used as a lake pigment is 1,2-dihydroxyanthraquinone (1,2-HAQ), also known as alizarin. Alizarin is produced naturally by multiple species related to *Rubia tinctorum* (common madder) where it is a primary chromophore along with 1,2,4-trihydroxyanthraquinone (1,2,4-HAQ), also known as purpurin.(*1*) It is well documented in the cultural heritage and condensed phase scientific communities that alizarin is more photostable than purpurin.(*8-11*) Condensed phase photodynamics studies of these AQs suggests that the difference in photostability may stem from an excited state pathway, specifically an excited state intramolecular proton transfer (ESIPT), in alizarin which dissipates photonic energy to regain a stable ground state structure on a timescale much faster than the reaction rates of degradation.(*11, 12*)

ESIPT constitutes one of the fastest reactions known,(*13, 14*) and planar organic molecules containing acidic and basic functional groups connected by an intramolecular hydrogen bond often have photophysics driven by such proton transfer. In such molecules, excited state tautomerization occurs through the excitation of the ground state enol-form to an electronically excited intermediate where a rapid (sub-picosecond timescale), often energetically barrierless, enol to keto proton transfer takes place. Radiationless decay follows this transfer, bringing the excited keto form back to the ground state, and the stable ground state enol reforms through a barrierless back proton transfer.(*15*) Molecules which undergo ESIPT are typically identified by dual band fluorescence with a large degree of Stokes shift from the ESIPT lower well equilibrium geometry.

Formative work examining this mechanism in AQs/HAQs was done in the 1980s (*16*); laser induced fluorescent spectroscopy studies (*17*), including by Flom and Barbara, (*15*) determined that the presence of a dual 1,4- electron donating group (e.g. -OH) precludes dual fluorescence, likely indicating a high barrier towards ESIPT. This qualitative result was later supported by the nodal-plane model by Nagaoka.(*18*) More recent transient spectroscopic work has measured the rate of ESIPT (*19-21*) as a femtosecond process and correlated this with pigment fading (*11, 22*). However these are all condensed phase experiments where the effects of secondary molecules, such as solvent molecules or other pigment components, cannot be completely excluded, which is particularly important since intermolecular effects are widely known to affect relaxation.(*20, 23*) To measure

the unimolecular dynamics of the AQ and HAQ molecules requires gas phase experiments. It should be noted that in the context of art materials, much of the available literature deals only with alizarin and purpurin as exemplars of the HAQ system.(*24*) Therefore, there remains a need to examine a broader range of these important molecules in the gas phase to fully explicate the observed differences in the relative photostabilities of the basic chromophores themselves. By studying a larger set of isolated HAQs it is possible to identify the key structural motifs that determine the photodynamics of this class of compounds and further explicate the observed photochemical behavior of alizarin and purpurin. Such a fundamental study can then inform a fuller understanding of the more complex systems found in works of art, which will include binding media, the support, and other pigments in addition to the organic red colorant in question.

In this paper, we address this need, and report an experimental and computational case study on the effects of proton transfer on the excited state lifetimes of seven related HAQs as isolated chromophores. We measured intrinsic lifetimes of a series of neutral HAQ molecules in a jet-cooled molecular beam by time resolved, pump-probe, two-color (2C) resonant two-photon ionization (R2PI) spectroscopy to elucidate the relaxation dynamics occurring at the lower limit of the excited state potential energy surface (PES). For each molecule studied, these data provide the first 2C R2PI action spectra, building a library to allow their identification in works of art. We also obtained the excited state lifetimes from both the lowest energy vibronic transition and at higher internal energy (~500-1000 cm^{-1}) and, for selected compounds, partial mid-IR characterization of the ground state hydrogen bond vibrations with IR hole burning of the R2PI probe signal. These measurements allow us to study these chromophores in selected unique tautomeric forms. The resulting detailed vibrationally and tautomerically resolved excited state lifetime data reveal the intrinsic properties of the chromophores and serve as the basis for high level quantum computational modeling of the excited state dynamics. We explore the implications of the resulting data for the photodegradation of these compounds. Our results show a trend of shorter excited state lifetimes for the structures for which there is evidence for ESIPT, as derived from dual fluorescence by Flom and Barbara and others. We find that both phenomena correlate with structural motifs with a specific double hydrogen bonding pattern and this observation provides experimental evidence to support predictions for the expected stability of HAQs beyond alizarin and purpurin in works of art.

Results

Analytes studied and R2PI spectroscopy

Fig. 1 shows the series of substituted HAQs analyzed. The analytes represent structures with and without the 1,4-OH substitution motif postulated to be determinative of ESIPT properties.(*11, 15*). Several of these molecules are also found in artists' red lake pigments. The molecular structures shown in Fig.1 are planar in all cases. In each molecule the lowest energy (LE) structure (indicated by the Roman numeral I) is that of the 9,10-anthraquinone, with carbonyl groups rather than hydroxyl moieties on the central ring of the backbone. The interpretation of R2PI and pump-probe spectra requires an understanding of the possible structures present in the molecular beam, which are most likely the lowest energy isomers. Fig. 1 shows all isomers with energies calculated to be within 25 kJ/mol of the lowest energy (LE) structure; isomeric forms with higher energies appear in the supplemental information. The center of Fig. 1 shows the two primary *common madder* chromophores alizarin (1,2-HAQ) and purpurin (1,2,4-HAQ). Both have multiple low energy isomers, as do 1,2,5,8-HAQ and 1,4-HAQ. Three of the molecules examined – 1-HAQ, 1,5-HAQ, and 1,8-HAQ – have only a single lowest energy structure (the rotamers for each of these molecules are 52.3, 53.2, and 47.4 kJ/mol higher in energy than the forms shown, respectively). In the figure

and throughout we use the nomenclature of HAQ for all compounds, ignoring the more formal designations of DHAQ and THAQ for the di- and trihydroxy forms, as the numbered prefixes already indicate the number of hydroxyl substituents.

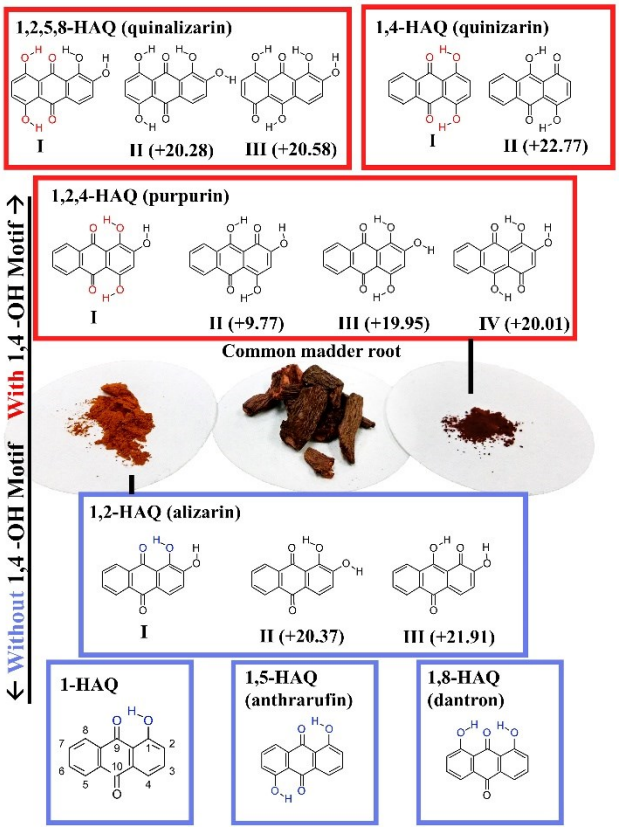

Fig. 1. The molecules of this study. Molecules having a 1,4 -OH motif are above the dotted line and those without 1,4 -OH motif are below it. Isomers within ~25 kJ/mol of the lowest energy ZPE corrected structure (labeled I) are also shown with their relative energy values (kJ/mol) with respect to the lowest energy form. Central to this figure is the common madder root and its primary chromophores alizarin and purpurin.

Fig. 2 presents the R2PI spectra of the HAQs from Fig. 1. The origins, corresponding to $S_{0\text{-}0}$ transitions, of molecules with a 1,4-motif are about 2000 cm^{-1} lower in energy than those without the 1,4-motif. The origins of 1,2,5,8-HAQ (19,661 cm^{-1}), 1,2,4-HAQ (19,845 cm^{-1}), and 1,4-HAQ (19,920 cm^{-1}) all lie within 300 cm^{-1} of each other, and each is characterized by sharp, laser linewidth limited, bands over a ~1000 cm^{-1} range. In contrast to this, the spectra for HAQs without the 1,4-motif are broader, suggesting shorter excited state lifetimes. Their origins – 1-HAQ (21,645 cm^{-1}), 1,2-HAQ (21,748 cm^{-1}), 1,5-HAQ (21,321 cm^{-1}), and 1,8-HAQ (22,031 cm^{-1}) – are located over a larger energy spread, though still within ~700 cm^{-1} of each other. The difference between these two groups of spectra, suggests that the excited state properties strongly depend on the presence or absence of the 1,4-OH structural motif.

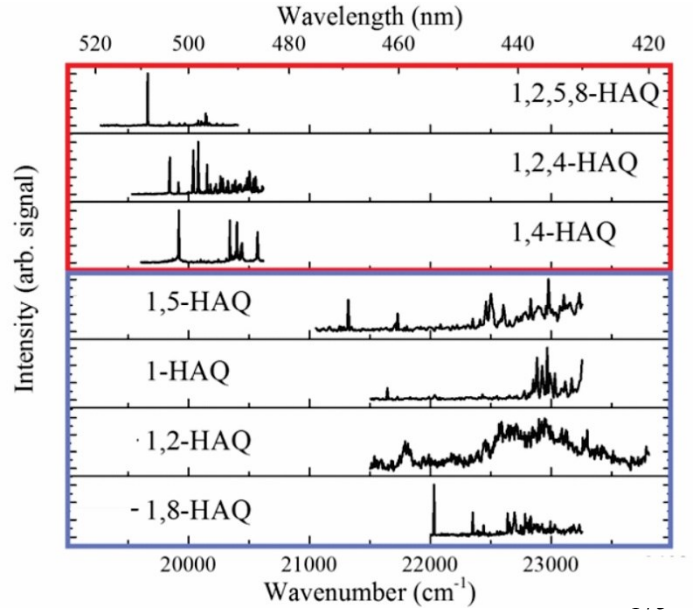

Fig. 2. Picosecond 2C-R2PI spectra of each HAQ in this study (OPG + 213 nm). Intensities have been normalized.

Pump-probe spectroscopy

We performed picosecond pump-probe measurements for each HAQ from Fig. 1 on both the origin transition and on one additional higher energy transition, determined from the R2PI spectra. The measurement using the higher energy transition probed whether additional relaxation pathways become available at higher energies, which would likely be evidenced by a change in excited state lifetime. Fig. 3 shows the effect of structure on excited state lifetime. The molecules with the 1,4-OH motif, shown at the top in Fig. 3a in a red box, have nanosecond lifetimes at their lowest energy transitions. In contrast, those molecules without the 1,4-OH motif, shown at the bottom of Fig. 3a in a blue box, have sub-nanosecond lifetimes.

Coincidently, the primary madder chromophores (1,2,4-HAQ and 1,2-HAQ) have the longest and the shortest excited state lifetimes, respectively, of all molecules measured. Fig. 3b shows the pump-probe traces of these two end-members (picosecond pump-probe data for the other molecules are shown in Fig. S1, Supplemental Information). Each of these traces can be adequately fit using a single exponential, providing the excited state lifetime of each molecule. When probed at the origin, 1,2,4-HAQ (purpurin) has an excited state lifetime of 5.4 ns, while 1,2-HAQ (alizarin) has an excited state lifetime of only 120 ps. Others of the HAQ series have lifetimes intermediate between these two: 1-HAQ has a measured lifetime of 290 ps while 1,4-HAQ has a measured lifetime of 1.7 ns, for example. In general, excitation at higher energies shortens the lifetime, as shown in Fig. 3a (black bars). 1,4-HAQ provides an exception to this trend, with a slight increase in excited state lifetime when measured at a transition +655 cm^{-1} from the origin (from 1.7 ns to 1.9 ns). This slight increase is likely an artifact due to the short observation period relative to the excitation lifetime. For completeness, we also carried out nanosecond pump-probe measurements on the two endmembers (1,2,4-HAQ and 1,2-HAQ, data shown in Fig. S2). These measurements show no component at longer time scale than those found in the ps measurements.

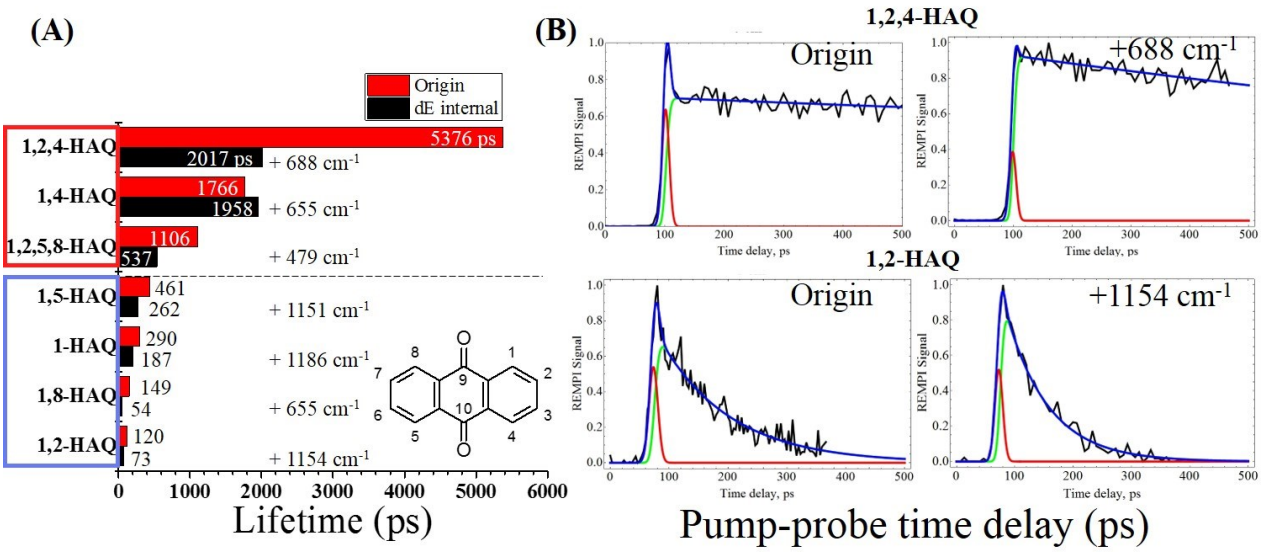

Fig. 3. Results of picosecond pump-probe spectroscopy. (A) Pump-probe lifetime as measured at the origin transition (red bars) and at excess energy (black bars), arranged in order of decreasing measured lifetimes. The excess energy transition used is noted next to the black bars. (B) Pump-probe traces of the molecules with the longest and shortest measured excited state lifetime, 1,2,4-HAQ and 1,2-HAQ respectively, plotted over 500 ps. The pump-probe data are fit to a curve (blue trace) which is the sum of a single exponential decay (green trace) convolved with a Gaussian component (red trace) representative of our instrument response function (IRF).

Intramolecular Hydrogen Bonding Characterization and Structural Confirmation

In order to understand the hydrogen bonding environment of the isomer of species in the molecular beam with and without the 1,4-OH motif, we performed IR hole burning. IR-UV results in mode II indicate that for 1,2,4-HAQ and 1,4-HAQ the R2PI results are from a single conformation (see Supplemental Information Fig. S3).

We also performed hole burning in mode I on 1,2,4-HAQ, 1,4-HAQ, and 1,8-HAQ while probing the origin of each, as shown in Fig. 4. In all three spectra the peak at ~3,100 cm^{-1} represents stretching modes associated with the -OH hydrogen bound to a carbonyl group. In the case of 1,8-HAQ this peak is broadened by the competitive sharing of the carbonyl with intramolecular hydrogen bonds 180° about the oxygen atom (9-position). In the case of 1,2,4-HAQ the peak at 3570 cm^{-1} results from the in-plane hydroxyl (2-position) which is hydrogen bound to the neighboring hydroxyl (1-position). The 470 cm^{-1} separation is a direct measurement of different hydrogen bond environments: between carbonyl and hydroxy intramolecular bonded -OH stretches.

Fig. S4 in supplemental information also shows calculated LE spectra convoluted with a lorentzian linewidth of 3 cm^{-1}. These calculations reproduce the experimental patterns but not the exact frequencies, reflecting the fact that these are unscaled harmonic calculations. Future work with anharmonic calculations at a higher level may provide further details on structures.

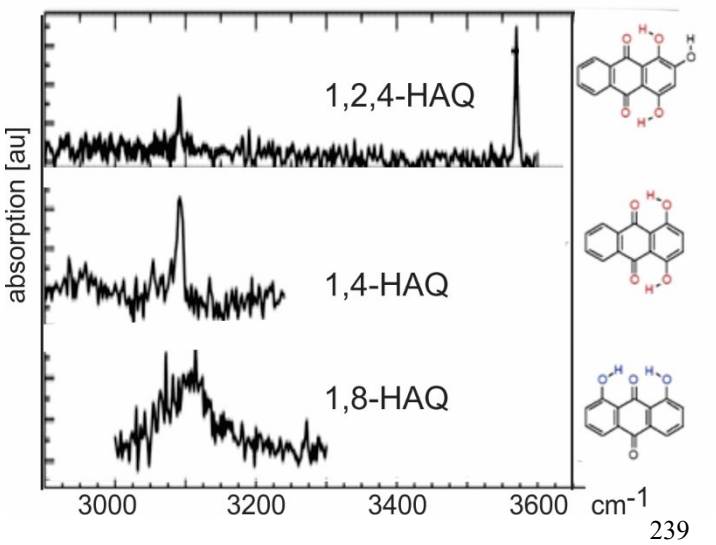

Fig. 4. IR hole burning spectra. Spectra were taken in mode I of 1,2,4-HAQ, 1,4-HAQ, and 1,8-HAQ probed at their origin R2PI transition.

Theoretical calculations: 1-HAQ and 1,4-HAQ

To model computationally the difference in excited state dynamics in the two structural motifs, with and without the 1,4 substitution, we performed detailed calculations on the most basic representatives of the two structural families, namely 1-HAQ and 1,4-HAQ.

1-HAQ: ground and excited state

Fig. 5 shows the calculated energetic landscapes of 1-HAQ. The ground-state global minimum of the keto form (I in Fig 5, hereafter referred to as K(I)) with the proton attached to the O_1 oxygen atom, is planar and stabilized by a single intramolecular hydrogen bond between two oxygen atoms as proton acceptor: O_1-H…O_9. The proton transferred form (enol form, II in Fig. 5, hereafter referred to as E(II)) with the proton attached to the O_9 oxygen atom is not stable in the S_0 state, and its geometry optimization transfers the proton back to the O_1 oxygen atom to reform the global minimum, form K(I). Possible rotation of the O_1H group could generate the second lowest S_0-state minimum, the keto rotamer (III in Fig. 5) structure. However, the O_1H rotation breaks the intramolecular hydrogen bond in the 1-HAQ structure, which destabilizes the rotated form compared to the global minimum K(I) by 0.52 eV (50 kJ/mol). Furthermore, the rotamer (III) minimum is separated from the global minimum by a S_0-state energy barrier of 0.16 eV (15kJ/mol). The fourth form, IV with the proton attached to the O_9 atom, has much higher energy and can be excluded from this study. This energetic profile indicates that the 1-HAQ molecule should exist in the K(I) form in the ground state.

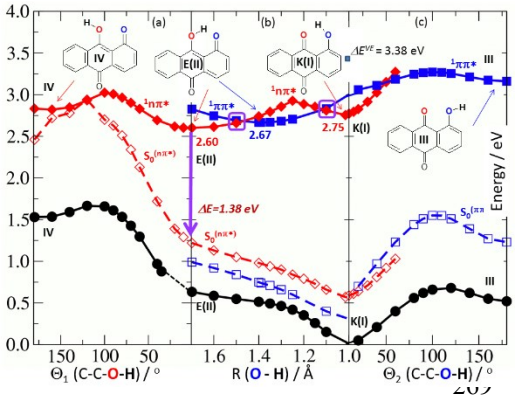

Fig. 5. Potential-energy energy profiles of 1-HAQ. Profiles shown are of the S_0 state (black circles), the $S_1(\pi\pi^*)$ state (blue squares) and the $S_1(n\pi^*)$ state (red diamonds) of the 1-HAQ molecule as a function of the torsional reaction path (a, c) and the hydrogen-transfer reaction path (b). Full lines (full symbols): energy profiles of reaction paths determined in the same electronic state. Dashed lines (empty symbols) represent ground-state energy calculated for the geometry optimized in the given excited state $n\pi^*$(red) or $\pi\pi^*$ (blue). Purple rectangles highlight the $n\pi^*$ and $\pi\pi^*$ intersections.

When 1-HAQ is irradiated, the ground-state K(I) form is photo-excited to the lowest ππ* excited state, $S_2(\pi\pi^*)$ with vertical energy ΔE^{VE} =3.38 eV at the S_0-state minimum geometry. At this optimized ground-state geometry of K(I), S_1 is a dark nπ* state below the $S_2(\pi\pi^*)$. The lowest ππ* excited state does not have a stable minimum in the K(I) form. Therefore, as long as the system remains in the excited ππ* state, the proton will transfer between the two oxygen atoms (from O_1 toward O_9) along a barrierless path to form the proton-transferred ππ* excited-state form, E(II), as indicated by the minimum of the blue curve (full squares) in the central panel of Fig. 5.

As depicted in Fig. 5 (highlighted with purple rectangles), the nπ* and ππ* excited states intersect in the vicinity of the $S_1(\pi\pi^*)$ state minimum, E(II). Consequently, the nπ* state can be populated directly from the ππ* excited state. The nπ* state has two minima, at the K(I) and E(II) forms, and the adiabatic energies of both minima are lower than that of the $S_1(\pi\pi^*)$ E(II) minimum. Once in the non-fluorescent nπ* state the system seeks another decay channel. The S_1-S_0 energy gap lowers for the nπ* state to 1.38 eV for the E(II) excited-state form, as depicted by the vertical purple line in Fig 5. As shown in Fig. 5, if the system is in nπ*- E(II) minimum, rotation of the O_9H group may lead to further significant decrease of the S_1-S_0 energy gap (see red traces) until S_1 and S_0 meet at a C-C-O_2-H dihedral angle of about 100 °. This pathway provides an additional channel for excited-state deactivation. However, the large barrier in the nπ* excited state may make this process less efficient.

1,4-HAQ: ground and excited state

The addition of the OH group to position 4 of the 1-HAQ molecule (that is, the introduction of the 1,4-OH motif) results in significant changes, both structurally by forming a second intramolecular hydrogen bond, and photo-physically by changing the ordering of the excited states.

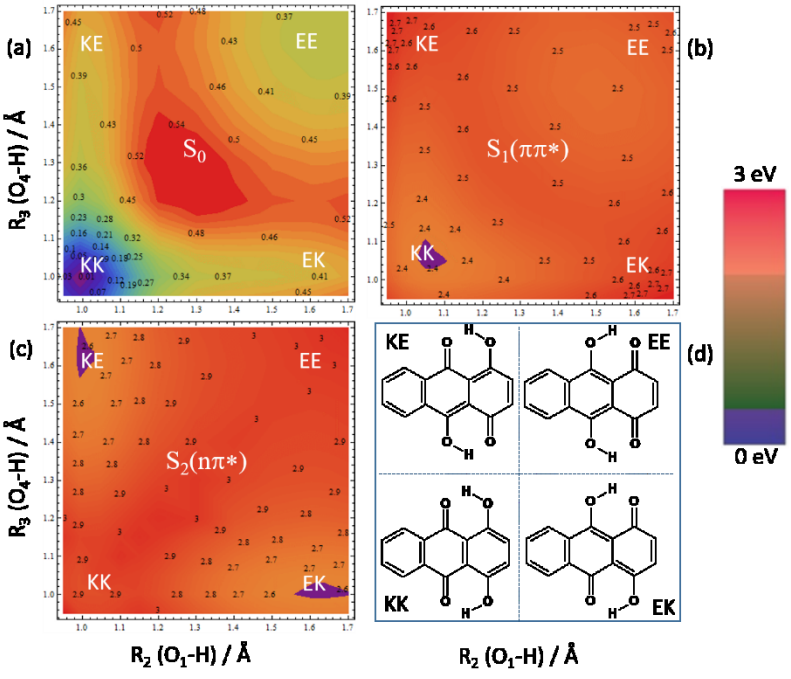

Fig. 6. Potential energy surfaces (PES) of 1,4-HAQ. (a) Minimum PES of the S_0 state, (b) the $S_1(\pi\pi^*)$ singlet excited state, (c) the $S_1(n\pi^*)$ singlet excited state of the **1,4-HAQ** molecule as a function of the hydrogen-transfer reaction path as a function of two coordinates: R(O_1….H) and R(O_4…H). (d) Schematic indication of the structures at the four combinations of minimum and maximum R values. The location of each tautomer on the PES are also labeled.

.

In contrast to 1-HAQ, 1,4-HAQ possesses two intramolecular hydrogen bonds: O_1-H…O_9 and O_4-H…O_{10} which bridge the molecule on opposite sides and ensure planarity of the system. Fig. 6 displays the 2-dimensional PES of 1,4-HAQ, with panels (a), (b), and (c) showing the S_0, S_1 and S_2

states, respectively; panel (d) illustrates the possible tautomers of 1,4-HAQ, both single hydrogen transfers (KE and EK), and double hydrogen transfer (EE). The x-axes of Fig. 6(a-c) are the reaction coordinate for the hydrogen displacement from O_1 while the y-axes are the reaction coordinate for the hydrogen displacement from O_4. Moving along the x-axis moves the hydrogen from O_1 to O_9 while the y-axis moves the hydrogen from O_4 to O_{10}. Thus, the top right corner of each energy surface is the EE tautomer, the product of both hydrogen transfers. There exists a tautomer in each corner of each PES, labeled accordingly. In addition to the global minimum form – the KK form with protons attached to O_1 and O_4 – the EE form, with the protons attached to O_9 and O_{10}, provides an additional local minimum, 0.36 eV higher in energy. As shown in Fig. 6a, the EE minimum is separated from the KK form by relatively small S_0-state energy-barrier of ~ +0.15 eV. The presence of this additional stable tautomer and the energy barrier (in contrast to the 1-HAQ system which lacks an energy barrier) might be explained by the fact that any proton transfer usually requires shortening of the interatomic distance between two proton accepting centers (here, two oxygen atoms). While one interatomic distance, e.g. $O_1 \ldots O_9$, contracts, the other, i.e. $O_4 \ldots O_{10}$, must simultaneously lengthen. This effect is not energetically favorable, creating the barrier in S_0.

In these coordinates for the ππ* (Fig. 6b), the KK tautomer is the minimum by ~0.15 eV. A single or double proton transfer to generate any other tautomer would be uphill and unfavorable. The vertical excitation energies, ΔE^{VE}, to the lowest excited ππ* state of the KK and EE forms of the 1,4-HAQ molecule are: 2.80 eV and 2.58 eV, respectively (for a complete tabulation of results, see Tables S1 and S2, Supplemental Information). Both ΔE^{VE} values for 1,4-HAQ are lower than the respective value of 3.38 eV for 1-HAQ which is consistent with the experimental pattern of the origin shifts. This effect is consistent with π-electron donating character of the OH group(*25*) which should result in stabilization of the ππ* excited state *vs* the nπ* state for a given structure. Indeed, the lowest nπ* states (Fig. 6c) in the absorption ladder of both tautomeric forms of 1,4-HAQ are at least 0.5 eV above the lowest ππ* states and therefore inaccessible.

The properties of the optimized excited state forms of the molecule are gathered in Table S1. KK and EE, respectively, each have the same ground state and ππ* excited state geometries. Both excited-state forms are almost isoenergetic. Moreover, a barrier of only 0.15 eV separates the S_1 states of these two forms. At the same time, the nπ* state PES lies almost entirely above the fluorescent ππ* state. Such a situation greatly reduces the probability for nonradiative decay for the 1,4-HAQ in comparison to the 1-HAQ system.

Discussion

The experimental and computational results from this series of molecules demonstrate that the presence or absence of a hydroxyl substitution at the 4 position has profound effects on the spectroscopy and dynamics of substituted anthraquinones.

When interpreting spectral and pump-probe results it is important to keep in mind that multiple tautomeric forms are possible (as shown in Fig. 1). Generally, in jet-cooling conditions only the lowest energy forms exist and the mode II IR-UV data for 1,2,4-HAQ and 1,4-HAQ suggest those data to be exclusively from a single tautomer (though it is possible that signal arises from complimentary rotamers in Fig. 1). We assume the other compounds also to be exclusively or at least predominantly in the lowest energy tautomeric form but the possible existence of other tautomers in the beam cannot be definitively excluded.

With this limitation in mind, the experimental and computational evidence can be summarized as follows: (i) The origin transition for HAQs with the 1,4-motif is about 2000 cm^{-1} to the red of those

without the 1,4-motif, as shown in Fig. 2.(ii) The excited state lifetime is approximately an order of magnitude shorter for those without the 1,4-motif, going from a few ns to a few hundred ps at the origin transition, as shown in Fig. 3. Relative to the 1-OH motif there is a 15× average longer lifetime for the molecular species with the 1,4-OH motif. (iii) In systems without the 1,4 motif (and therefore with short excited state lifetimes), proton transfer between the two oxygen atoms to form the proton-transferred ππ* excited-state form is likely, while systems with the 1,4 motif more energetically favorable forms are likely to be present, limiting the probability for nonradiative decay pathways.

The photobleaching effects of *common madder* chromophores, 1,2,4-HAQ and 1,2-HAQ, was recently investigated by Tan et al. by counting emissive events in time (photo-blinking) of these dyes under inert (N_2) irradiant conditions on glass. They measured that alizarin is able to absorb and emit four times longer (and over many more events) than purpurin, which they argue to be due to a long lived excited state of purpurin which degrades through electron injection to the glass slide.(*11*) This decay pathway is consistent with the literature.(*19, 21, 26, 27*) One cannot compare absolute lifetime values between gas phase and condensed phase states but the trend in the condensed phase correlates with the inherent lifetime trends presented here that 1,2-HAQ is ~ 45 times shorter lived at its vibrationless transition than 1,2,4-HAQ. The experimental data presented here seem to suggest that this pathway may be common to other substituted HAQs, with variations in the excited state lifetimes determined by the exact substitution arrangement.

Our theoretical investigation focused on the excited state potentials of 1-HAQ and 1,4-HAQ, since the experimental work showed that these motifs represent two distinct families of molecules. For 1-HAQ, the computations explain the experimentally observed short lifetimes by an energetically downhill process from the initially populated ππ* state. Along the proton transfer coordinate, the nπ* state is crossed twice, leading to the minimum of E(II). Following this pathway, the energy gap to the ground state is 1.38 eV, allowing for nonradiative decay, although there may be additional involvement of an out of plane torsion, leading to a conical intersection. These dynamics are consistent with the relatively short lifetimes observed for the HAQs without a 1,4-motif. After reaching the ground state, it is a downhill path to transfer the proton back and complete the photocycle, recovering the K(I) tautomer.

The addition of the OH group to the 4 position of the HAQ skeleton results in several critical changes to ground and excited state profiles. First, in the 1,4-HAQ molecule there is a second S_0 state minimum, the EE characterized by the two protons being transferred to the oxygens on carbons 9 and 10. Additionally, the shape of the ππ*-excited state in 1,4-HAQ is much shallower than in 1-HAQ and photoexcitation of the KK form does not result in a barrierless proton transfer to the EE form as in 1-HAQ. The most prominent effect is that the ππ* excited-state PES lies below the nπ* excited-state PES, an effect of electron-donating property of the OH-group, which tends to stabilize the ππ* excited state versus the nπ*state. This explains the red shift of 1,4 motif versus those molecules that lack it (*25, 28*). Due to the stabilization of the ππ*, the nπ* is not accessible at the excitation energies utilized. This effect inhibits non-radiative decay from the excited ππ* to S_0 via crossing to the nπ*, as is the case for 1-HAQ. A major effect of 4-OH substitution is related to the unique stabilization of the KK(ππ*), lacking the downhill proton transferred minimum of the ππ* excited state in 1-HAQ. The analogous initial ππ* state in 1-HAQ undergoes proton transfer in a barrierless manner, leading to ps excited state lifetimes. However, this proton transfer shortens the interatomic distance between the two proton accepting oxygen atoms. With the 1,4 motif, while one interatomic distance, e.g. O1…O9, contracts, the other, i.e. O4…O10, simultaneously lengthens, creating a barrier in the excited state potential. As a result, we find a single ns timescale lifetime for the molecules with a 1,4-motif, implying that instead of undergoing ESIPT, they relax

from the initially populated ππ* state. This model also explains why 1,5-HAQ and 1,8-HAQ – both doubly hydrogen bound – behave photodynamically like 1-HAQ.

We investigated the possibility of longer-lived states such as triplets with a ns ionization source for 1,2-HAQ and 1,2,4-HAQ, but have not observed such states experimentally. However, Mohamed et al. reported formation of a long lived triplet state with high quantum yield in a study of 1,8-HAQ in a series of nonpolar, polar aprotic, and polar protic solvents.(*20*) Further work in this area is therefore justified to clarify whether long lived triplets may form in some systems.

As seen by Flom and Barbara and explained by Nagaoka et al., the 1-HAQ motif exhibits dual fluorescence due to ESIPT. As the main excited-state pathway, this explains the photostability of molecules lacking the 1,4-HAQ motif observed in works of art (by, e.g. alizarin). In contrast, molecules **with** the 1,4-HAQ motif lack dual fluorescence and the corresponding ESIPT properties. At the same time, molecules with the 1,4-HAQ motif are noted for their photodegradation in works of art (e.g. purpurin). We have corroborated these phenomena both experimentally and theoretically in the gas-phase, indicating that this is a fundamental characteristic of the anthraquinone molecules used to create lake dyes, and not due to other effects such as interactions with the substrate on which the dyes are precipitated, the binding media or other pigments that may be present in the complex system of a work of art. Molecules with the 1-HAQ motif have ~15x shorter excited state lifetime than molecules with the 1,4-HAQ motif, explaining the former's photostability. The energetically downhill process of ESIPT accounts for the shorter lifetime of the 1-HAQ motif. Meanwhile, the geometries resulting from ESIPT of the 1,4-motif are all higher in energy than the initially excited, non-proton transfer state, making PT highly unfavorable. Without this process available, the 1,4-motif has a much longer excited-state lifetime and worse photostability.

Taken with the body of work done on UV radiation on anthracene by Mallakin on the production of toxic species (i.e. reactive, typically $^1O_2$) through the stepwise formation and further irradiation of AQs and HAQs (*29, 30*) and the work by Nagaoka et. Al (*18*) on the quenching of singlet oxygen ($^1O_2$) by ESIPT HAQs, and the previous experimental and theoretical work done on alizarin and purpurin (*8-12, 27*), the data presented here form a complex picture of the degradation of the madder colorants – and anthraquinone dyes more generally – in cultural heritage materials. These pigments need a way to dissipate photoenergy that they inherently will absorb from the environment. But without a viable energetic channel for decay, such as proton transfer or quenching of singlet oxygen, anthraquinone chromophores with a 1,4- substitutional motif will tend to degrade at a faster pace than their photostable counterparts which lack this motif. Knowledge of the structural trend that drives the photochemical response, therefore, allows those who care for culturally significant materials to better predict their photosensitivity: if the specific chemical composition of the organic red dyes in an object can be determined, and a 1,4- substitutional motif is prevalent (either in the only chromophore present, or in high concentration in a mixture of several anthraquinones), a higher photosensitivity can be presumed than if the structure were lacking, regardless of how many chromophore(s) are present. The data shown here suggests that conservators and curators may therefore use information about the chemical structure to predict general trends in the photosensitivity of the objects in their care if colored with anthraquinone dyes, and protect those objects accordingly.

Materials and Methods

Experimental Design

Standards of seven HAQs were purchased from Sigma-Aldrich and used without further purification. Standards were directly applied to individual graphite sample bars as a thin solid layer and examined in isolation to ensure spectral purity for 2C-R2PI and pump-probe measurements.

The instrument has been previously described in detail and only a brief description of the experimental setup follows.(*31, 32*) Samples are laser desorbed in vacuo directly in front of a pulsed molecular beam controlled by a piezo cantilever valve.(*33*) The desorption laser is a tightly focused Nd:YAG laser (1064 nm, ~ 1 mJ/pulse) and the piezo cantilever valve operates at a 45 μsec pulse duration with 8 bars backing argon gas. The desorbed sample is adiabatically cooled by collisions with the argon jet-expansion to between 10-20 K and the molecular beam is skimmed before being intersected by laser beams and photo-ionized by two-color resonant two photon ionization (2C-R2PI). The subsequent ions are detected by a reflectron time of flight mass spectrometer (2×10^{-6} Torr analyzer pressure, mass resolution $m/\Delta m=500$).

The 2C-R2PI spectroscopic and picosecond (ps) pump-probe delay measurements are performed with an Ekspla PL2251 Nd:YAG laser system producing ~30 ps laser pulses. The 355 nm output pumps an Ekspla PG401 tunable optical parametric generator (OPG) (VIS output of 450-600 uJ/pulse, ~6 cm^{-1} spectral linewidth). The sample is excited by the OPG and ionized by 213 nm, fifth harmonic of the Ekspla PL2251 laser, which is mechanically delayed up to 600 ps before colineation with the OPG beam. A variable electronic (SRS DG645) delay between OPG UV laser and an excimer laser (193 nm, 1.5-2 mJ/pulse) is used for pump-probe measurements in the nanosecond (ns) time delay range.

For IR-UV double resonant spectroscopy (i.e. IR hole-burning) a Laser Vision optical parametric oscillator/amplifier (OPO/OPA) (mid-IR output over the range 3,000-3,600 cm^{-1} of ~3-5 mJ/pulse, 3 cm^{-1} spectral linewidth) precedes the REMPI by 200 ns. This study utilized double resonant spectroscopy with two different pulse sequences: in mode I, the IR pump is scanned at a fixed UV probe wavelength, while in mode II, the UV is scanned with a fixed IR burn wavelength. In mode I, the UV laser wavelength is selected to correspond to a single vibronic transition, and the resulting 2C-R2PI signal depletes when the IR laser becomes resonant with the ground state population. The resulting ion-dip spectrum therefore represents the ground state IR spectrum of a single tautomer, selected by the UV probe wavelength. This IR spectrum can be compared with calculated IR frequencies to determine the specific tautomer of the selected vibronic transition. In mode II, the IR laser wavelength is selected to correspond to a tautomer-specific vibrational resonance, and spectra are collected both with IR laser on and off. The difference spectrum identifies peaks in the UV spectrum that arise from the same tautomer.

Calculations for IR-UV double resonant spectroscopy

Calculations were performed with the Gaussian 09 program package.(*34*) Starting structures for hydroxy derivatized anthracene-9,10-dione (HAQ) structures, tautomer and rotamer isomers, were optimized using the B3LYP hybrid functional with CC-pVTZ basis set. Relative zero- point corrected energy (ZPE) values are used to predict the number of isomers in our molecular beam based on the rule of thumb that for a given species isomers up to 20 kJ/mol of the lowest energy structure are typically kinetically trapped laser desorption jet-expansion. Past work on the nucleobase adenine showed that only the lowest energy isomer was present, where the next lowest energy isomer was calculated to be at ~33 kJ/mol higher energy than the one observed.(*35*) Ground state minima were confirmed by the absence of imaginary frequencies and these geometries were later used to determine electronic transition state strengths for S1-4 by way of TD-DFT with the B3LYP hybrid functional with CC-pVTZ basis set. The simulated IR spectra arise from frequencies with harmonic intensities using a Lorentzian shape and FWHM of 3 cm^{-1} and are presented without a spectral shift.

Calculations for construction of energy profiles

The ground-state minima forms of the 1-HAQ and 1,4-DHAQ were optimized by means of the MP2 method (*36*) using the cc-pVDZ(*37*) correlation-consistent atomic basis set. The excited-state geometries were optimized with the use of the same basis set while using the CC2(*38, 39*) method as implemented in TURBOMOLE software package (*40*). In the calculation of the vertical excitation energies, ΔE^{VE}, mimicking the absorption spectra, performed on top of the MP2/cc-pVDZ-optimized S_0-state geometries, the CC2(*38, 39*) method was used to evaluate the response properties.

To elucidate the photophysical mechanism on the molecular level the important driving coordinates were appropriately chosen for each system so that the ground– and the excited–state minimum potential–energy (MPE) profiles or surfaces could be constructed to estimate the ground– and excited–state energy barriers determining the photophysics of the both molecules. The 1-HAQ molecule is bound by a single hydrogen bond. In such case one coordinate – the $R_1(O_1H)$ distance – is needed to be chosen as a driving coordinate to illustrate the photophysical mechanism of the photo–tautomerization process. The MPE profile for 1-HAQ is constructed in a way that for fixed given value of the $R_1(O_1H)$ distance, all the remaining nuclear degrees of freedom are optimized; once in the ground state and twice in the two excited states: $S_1(\pi\pi^*)$ and $S_1(n\pi^*)$.

The 1,4-DHAQ system has an additional intramolecular hydrogen bond binding the molecule and more tautomeric forms are possible to be formed upon photoexcitation. A convenient method for illustrating the tautomerization process in such molecule is to construct the MPE surface spanning the two driving reaction coordinates describing the two intramolecular hydrogen bonds by the $R_2(O_2H)$ and $R_3(O_4H)$ distances. In that case both the R_2 and R_3 coordinates are being frozen for given values, while the rest of the parameters are being optimized in the constructed MPE surface, separately for the ground (S_0) and the two excited states: $S_1(\pi\pi^*)$ and $S_1(n\pi^*)$ with the C_s symmetry constrain.

References and Notes

1. J. Hofenk de Graaff, *The Colourful Past: Origins, Chemistry, and Identification of Natural Dyestuffs*. (Archetype Publications, London, 2004).
2. A. V. Whitney, R. P. Van Duyne, F. Casadio, An innovative surface-enhanced Raman spectroscopy (SERS) method for the identification of six historical red lakes and dyestuffs. *J. Raman Spectrosc.* **37**, 993-1002 (2006).
3. J. P. Brown, A review of the genetic effects of naturally occurring flavonoids, anthraquinones and related compounds. *Mutation Research/Reviews in Genetic Toxicology* **75**, 243-277 (1980).
4. E. M. Malik, C. E. Müller, Anthraquinones As Pharmacological Tools and Drugs. *Medicinal Research Reviews* **36**, 705-748 (2016).
5. M. J. Melo, A. Claro, Bright Light: Microspectrofluorimetry for the Characterization of Lake Pigments and Dyes in Works of Art. *Acc. Chem. Res.* **43**, 857-866 (2010).
6. C. L. Brosseau, F. Casadio, R. P. Van Duyne, Revealing the invisible: using surface-enhanced Raman spectroscopy to identify minute remnants of color in Winslow Homer's colorless skies. *J. Raman Spectrosc.* **42**, 1305-1310 (2011).
7. J. E. Fieberg, P. Knutas, K. Hostettler, G. D. Smith, "Paintings Fade Like Flowers": Pigment Analysis and Digital Reconstruction of a Faded Pink Lake Pigment in Vincent van Gogh's Undergrowth with Two Figures. *Appl Spectrosc* **71**, 794-808 (2017).
8. D. Saunders, J. Kirby, Light-Induced Color Changes in Red and Yellow Lake Pigments. *National Gallery Tech. Bull.* **15**, 79-97 (1994).
9. C. Clementi, W. Nowik, A. Romani, F. Cibin, G. Favaro, A spectrometric and chromatographic approach to the study of ageing of madder (Rubia tinctorum L.) dyestuff on wool. *Anal. Chim. Acta* **596**, 46-54 (2007).
10. C. Grazia, C. Clementi, C. Miliani, A. Romani, Photophysical properties of alizarin and purpurin Al(III) complexes in solution and in solid state. *Photochem Photobiol Sci* **10**, 1249-1254 (2011).
11. J. A. Tan *et al.*, Contributions from Excited-State Proton and Electron Transfer to the Blinking and Photobleaching Dynamics of Alizarin and Purpurin. *The Journal of Physical Chemistry C* **121**, 97-106 (2017).

12. C. Miliani *et al.*, Recent insights into the photochemistry of artists' pigments and dyes: towards better understanding and prevention of colour change in works of art. *Angew. Chem. Int. Ed.* **57**, 7324-7334 (2018).
13. A. Douhal, F. Lahmani, A. H. Zewail, Proton-transfer reaction dynamics. *Chemical Physics* **207**, 477-498 (1996).
14. S. J. Formosinho, L. G. Arnaut, Excited-state proton transfer reactions II. Intramolecular reactions. *Journal of Photochemistry and Photobiology A: Chemistry* **75**, 21-48 (1993).
15. S. R. Flom, P. F. Barbara, Proton transfer and hydrogen bonding in the internal conversion of S1 anthraquinones. *The Journal of Physical Chemistry* **89**, 4489-4494 (1985).
16. M. S. El Ezaby, T. M. Salem, A. H. Zewail, R. Issa, Spectral Studies of Some Hydroxy-derivatives of Anthraquinones. *J. Chem. Soc. B*, 1293-1296 (1970).
17. A. Navas Diaz, Absorption and emission spectroscopy and photochemistry of 1,10-anthraquinone derivatives: a review. *Journal of Photochemistry and Photobiology A: Chemistry* **53**, 141-167 (1990).
18. S.-i. Nagaoka, U. Nagashima, Effects of node of wave function upon excited-state intramolecular proton transfer of hydroxyanthraquinones and aminoanthraquinones. *Chem. Phys.* **206**, 353-362 (1996).
19. S. Lee, J. Lee, Y. Pang, Excited state intramolecular proton transfer of 1,2-dihydroxyanthraquinone by femtosecond transient absorption spectroscopy. *Current Applied Physics* **15**, 1492-1499 (2015).
20. O. F. Mohammed, D. Xiao, V. S. Batista, E. T. Nibbering, Excited-state intramolecular hydrogen transfer (ESIHT) of 1,8-dihydroxy-9,10-anthraquinone (DHAQ) characterized by ultrafast electronic and vibrational spectroscopy and computational modeling. *The journal of physical chemistry. A* **118**, 3090-3099 (2014).
21. M. Jen, S. Lee, K. Jeon, S. Hussain, Y. Pang, Ultrafast Intramolecular Proton Transfer of Alizarin Investigated by Femtosecond Stimulated Raman Spectroscopy. *J Phys Chem B* **121**, 4129-4136 (2017).
22. M. Smoluch, H. Joshi, A. Gerssen, C. Gooijer, G. van der Zwan, Fast excited-state intramolecular proton transfer and subnanosecond dynamic stokes shift of time-resolved fluorescence spectra of the 5-methoxysalicylic acid/diethyl ether complex. *J Phys Chem A* **109**, 535-541 (2005).
23. Y. Peng, Y. Ye, X. Xiu, S. Sun, Mechanism of Excited-State Intramolecular Proton Transfer for 1,2-Dihydroxyanthraquinone: Effect of Water on the ESIPT. *The journal of physical chemistry. A* **121**, 5625-5634 (2017).
24. M. Leona, J. Stenger, E. Ferloni, Application of surface-enhanced Raman scattering techniques to the ultrasensitive identification of natural dyes in works of art. *J. Raman Spectrosc.* **37**, 981-992 (2006).
25. M. F. Rode, A. L. Sobolewski, Effect of chemical substituents on the energetical landscape of a molecular photoswitch: an ab initio study. *The Journal of Physical Chemistry A* **114**, 11879-11889 (2010).
26. T. D. Giacco, L. Latterini, F. Elisei, Photophysical and photochemical properties of 1,2,4-trihydroxy-9,10-anthraquinone adsorbed on inorganic oxides. *Photochemical & Photobiological Sciences* **2**, 681-687 (2003).
27. A. Amat, C. Miliani, A. Romani, S. Fantacci, DFT/TDDFT investigation on the UV-vis absorption and fluorescence properties of alizarin dye. *Phys Chem Chem Phys* **17**, 6374-6382 (2015).
28. M. F. Rode, A. L. Sobolewski, Effect of chemical substitutions on photo-switching properties of 3-hydroxy-picolinic acid studied by ab initio methods. *The Journal of Chemical Physics* **140**, 084301 (2014).
29. A. Mallakin, D. George Dixon, B. M. Greenberg, Pathway of anthracene modification under simulated solar radiation. *Chemosphere* **40**, 1435-1441 (2000).
30. A. Mallakin *et al.*, Impacts of Structural Photomodification on the Toxicity of Environmental Contaminants: Anthracene Photooxidation Products. *Ecotoxicology and Environmental Safety* **43**, 204-212 (1999).
31. G. Meijer, M. S. Devries, H. E. Hunziker, H. R. Wendt, Laser Desorption Jet-Cooling of Organic-Molecules - Cooling Characteristics and Detection Sensitivity. *Appl Phys B-Photo* **51**, 395-403 (1990).
32. F. M. Siouri, S. Boldissar, J. A. Berenbeim, M. S. de Vries, Excited State Dynamics of 6-Thioguanine. *J Phys Chem A* **121**, 5257-5266 (2017).
33. D. Irimia *et al.*, A short pulse (7 micros FWHM) and high repetition rate (dc-5 kHz) cantilever piezovalve for pulsed atomic and molecular beams. *Rev Sci Instrum* **80**, 113303 (2009).
34. M. J. Frisch *et al.*, Gaussian 09, Revision B.01. (2009).
35. C. Plutzer, E. Nir, M. S. de Vries, K. Kleinermanns, IR-UV double-resonance spectroscopy of the nucleobase adenine. *Physical Chemistry Chemical Physics* **3**, 5466-5469 (2001).
36. C. Møller, M. S. Plesset, Note on an approximation treatment for many-electron systems. *Physical Review* **46**, 618 (1934).
37. T. H. Dunning Jr, Gaussian basis sets for use in correlated molecular calculations. I. The atoms boron through neon and hydrogen. *The Journal of chemical physics* **90**, 1007-1023 (1989).
38. O. Christiansen, H. Koch, P. Jørgensen, The second-order approximate coupled cluster singles and doubles model CC2. *Chem Phys Lett* **243**, 409-418 (1995).
39. C. Hättig, F. Weigend, CC2 excitation energy calculations on large molecules using the resolution of the identity approximation. *The Journal of Chemical Physics* **113**, 5154-5161 (2000).
40. R. Ahlrichs, M. Bär, M. Häser, H. Horn, C. Kölmel, Electronic-Structure Calculations on Workstation Computers - the Program System Turbomole. *Chem. Phys. Lett.* **162**, 165-169 (1989).

Acknowledgments

General: The authors thank K. Trentelman, B. Fonseca, J. Delaney, M. Fischer, M. Melo, and C. Miliani for helpful discussions.
Funding: This work was supported by the National Science Foundation under CHE-1800283. We acknowledge support from the Center for Scientific Computing from the CNSI, MRL: an NSF MRSEC (DMR-1121053) and NSF CNS-0960316.
Author contributions: J.B., S.B., S.O., M.R.H., G.G., F.M.S., T.C. (experimental work); J.B., S.B., M.F.R (computational work); C.S.P., M.S.dV (project development and funding); J.B., M.R.H., G.G., M.F.R, C.S.P., M.S.dV (manuscript preparation).
Competing interests: The authors have no competing interests.
Data and materials availability: All data needed to evaluate the conclusions in the paper are present in the paper and/or the Supplementary Materials. Additional data available from authors upon request.

Supplementary Materials

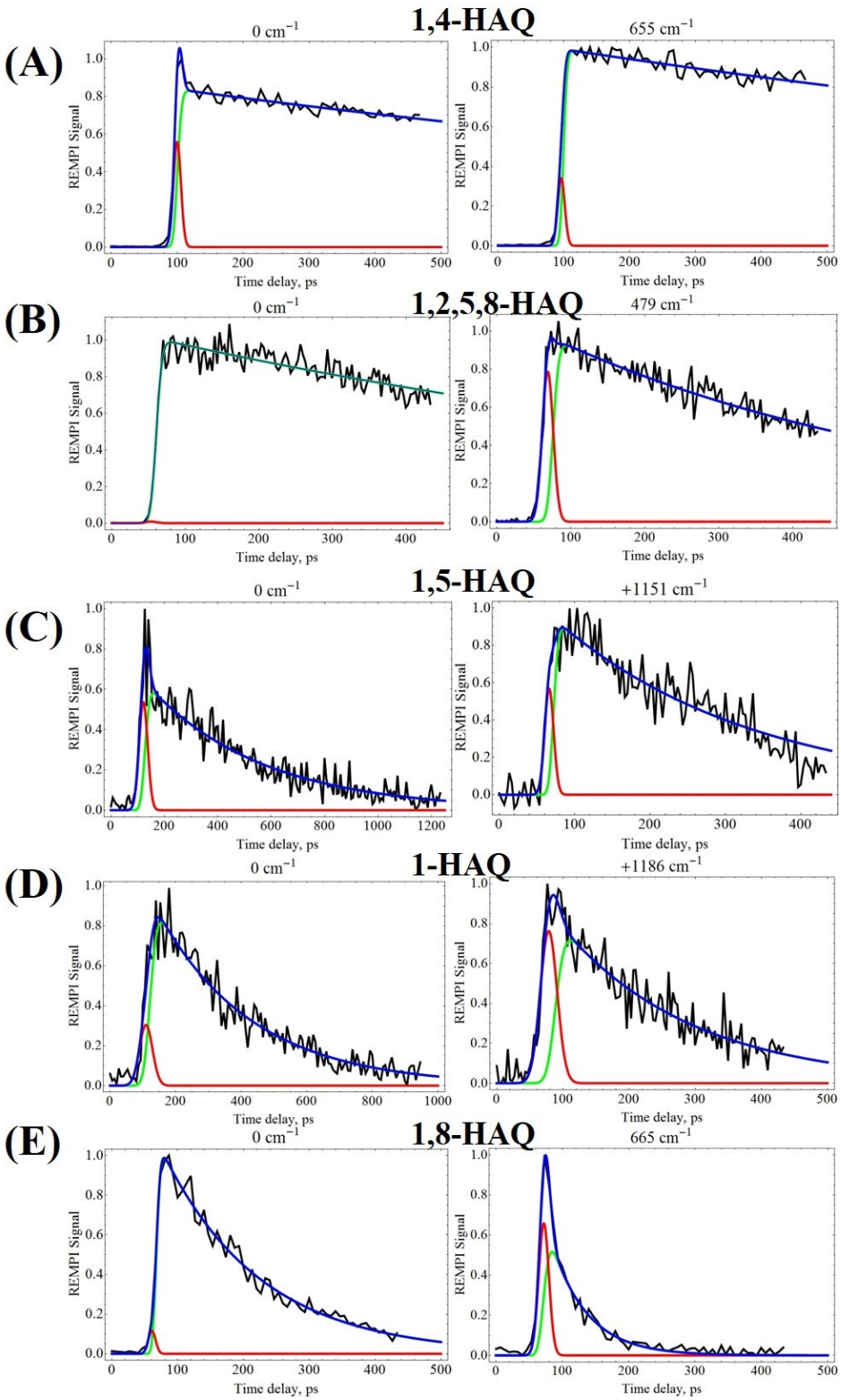

Fig. S1. Picosecond pump-probe spectra. (A) 1,4-HAQ, (B) 1,2,5,8-HAQ, (C) 1,5-HAQ, (D) 1-HAQ, and (E) 1,8-HAQ at vibrationless (left column) and excess probe lengths (right column). The pump-probe data are fit to a curve (blue) which is the sum of a single exponential decay convolved with a Gaussian component (red) representative of our instrument response function (IRF) the IRF itself (green).

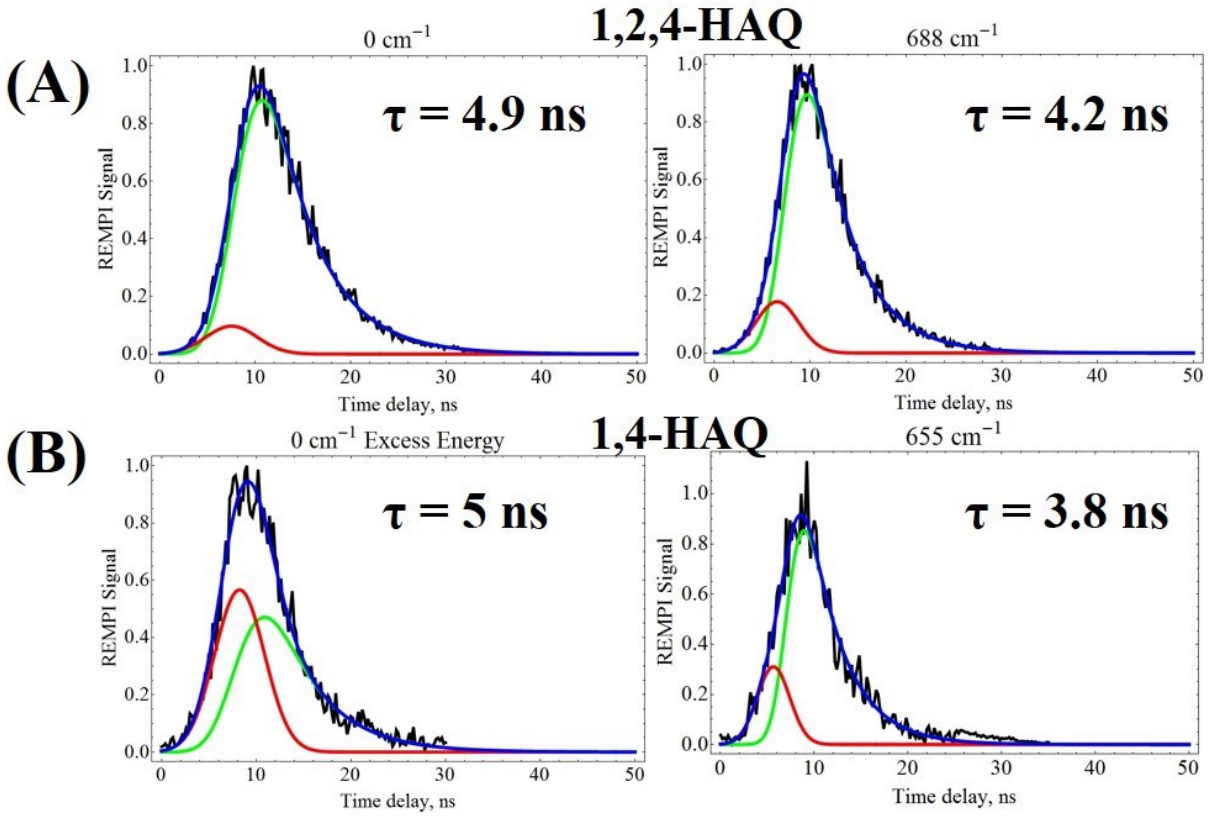

Fig. S2. Nanosecond pump-probe spectra. (A) 1,2,4-HAQ at vibrationless and excess probe lengths and for (B) 1,4-HAQ at vibrationless and excess probe lengths. The lifetime values here agree with those presented in Fig. 3for pump-probe measurement within the time jitter (± 3 ns) of the 193 nm ns ionization source. The pump-probe data are fit to a curve (blue) which is the sum of a single exponential decay convolved with a Gaussian component (red) representative of our instrument response function (IRF) the IRF itself (green).

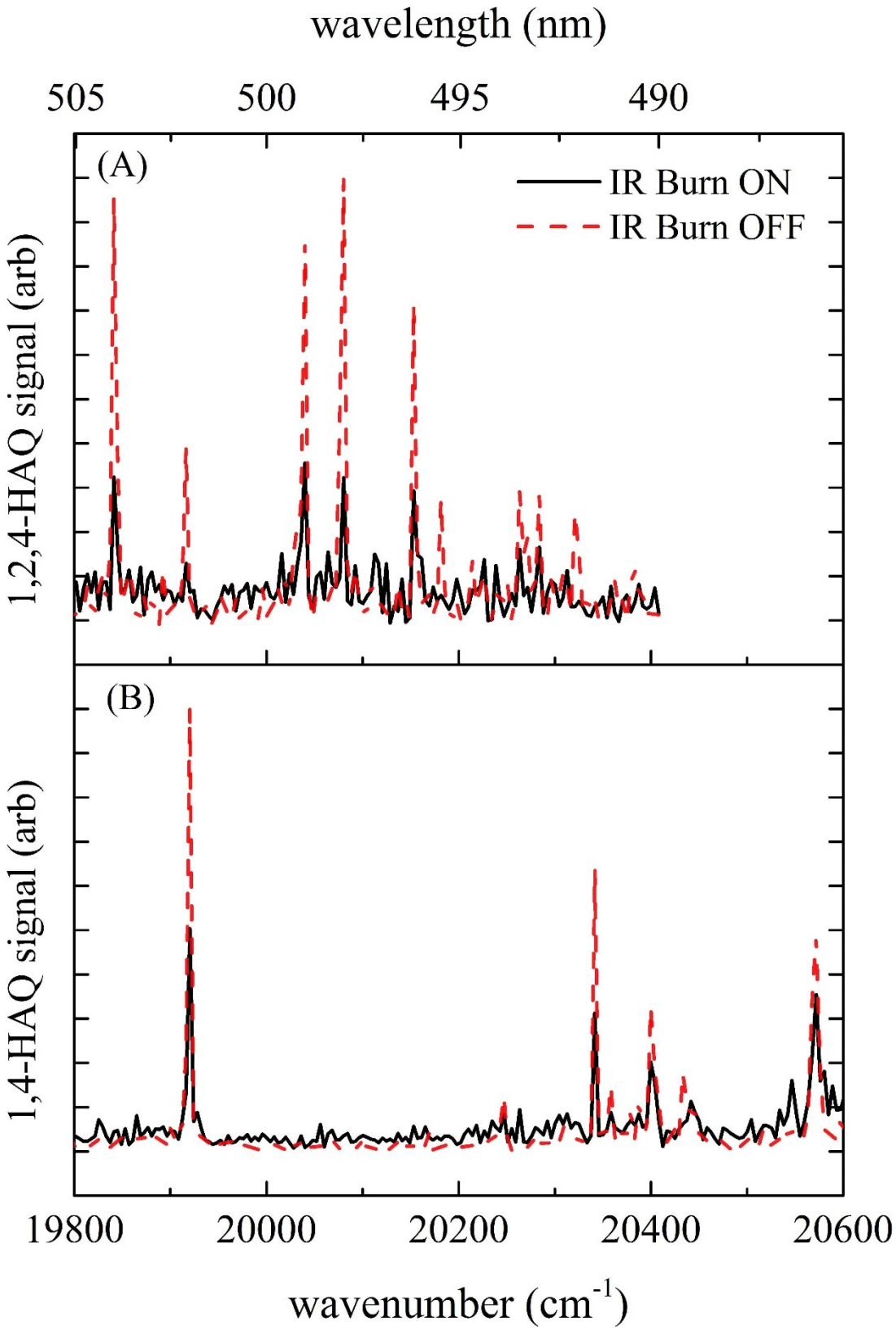

Fig. S3. IR hole burning spectra in mode II with the burn laser set to 3090 cm^{-1}. (A) All 1,2,4-HAQ vibronic transitions share resonance at IR burn wavelength, as do all (B) 1,4-HAQ vibronic transitions, suggesting a single tautomer in each R2PI spectrum.

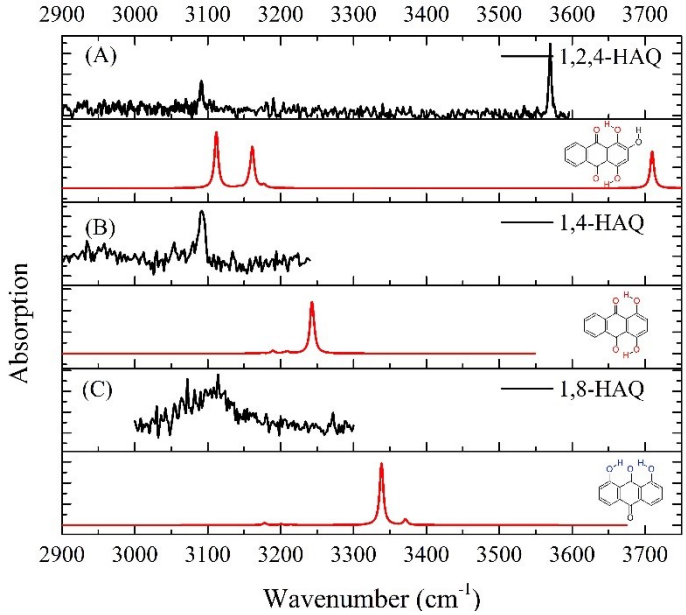

Fig. S4. IR hole burning spectra (in black) taken in mode I of (A) 1,2,4-HAQ, (B) 1,4-HAQ, and (C) 1,8-HAQ probed at their lowest energy R2PI transition. The ground state predicted frequencies for the given LE structure are plotted below each hole burn spectrum (in red). Harmonic analysis is shown unshifted.

Table S1: Calculated properties of 1-HAQ and 1,4-HAQ. Vertical excitation energies, ΔE^{VE} (in eV) for the stable minima of the **1-HAQ** and **1,4-HAQ** molecules calculated at the CC2/cc-pVDZ theory level at the geometries optimized with the MP2/cc-pVDZ method. The ground-state properties are marked Italic.

1-HAQ			
S_n / Tautomer	**ΔE^{VE} / eV**	***f***	**μ / D**
form K (I)			
S_0	*0.0*		*1.4*
$S_1(n\pi^*)$	3.21	0.000	2.8
$S_2(\pi\pi^*)$	**3.38**	**0.145**	4.4
$S_3(n\pi^*)$	3.62	0.000	2.6
$S_4(\pi\pi^*)$	4.28	0.029	4.9
$S_5(\pi\pi^*)$	4.31	0.012	1.3
$S_6(n\pi^*)$	4.97	0.000	4.0
form K_rot (III)			
S_0	*0.52*		*1.8*
$S_1(n\pi^*)$	3.10	0.000	3.6
$S_2(n\pi^*)$	3.43	0.000	2.2
$S_3(\pi\pi^*)$	**3.79**	**0.110**	7.2
$S_4(\pi\pi^*)$	4.34	0.035	3.2
$S_5(\pi\pi^*)$	4.55	0.014	0.7
$S_6(n\pi^*)$	4.74	0.000	6.3
1,4-HAQ			
S_n / Tautomer	**ΔE^{VE} / eV**	***f***	**μ / D**
form KK (I)			
S_0	*0.0*		*2.2*
$S_1(\pi\pi^*)$	2.80 (a1)	0.209	2.5
$S_2(n\pi^*)$	3.32 (b2)	0.000	1.9
$S_3(n\pi^*)$	3.65 (a2)	0.000	2.1
$S_4(\pi\pi^*)$	4.14 (b1)	0.000	0.4
$S_5(\pi\pi^*)$	4.29 (a1)	0.032	7.1
$S_6(\pi\pi^*)$	4.43 (b1)	0.006	4.0
form EE (II)			
S_0	*0.36*		*1.1*
$S_1(\pi\pi^*)$	2.58 (a1)	0.246	4.8
$S_2(n\pi^*)$	3.19 (b2)	0.000	0.6
$S_3(n\pi^*)$	3.46 (a2)	0.000	0.4
$S_4(\pi\pi^*)$	3.86 (b1)	0.007	0.9
$S_5(\pi\pi^*)$	4.16 (b1)	0.051	5.2
$S_6(n\pi^*)$	4.34 (a1)	0.002	4.2
form KK_rot (I)			
S_0	*0.55*		*0.9*
$S_1(n\pi^*)$	3.03	0.188	5.7
$S_2(\pi\pi^*)$	3.03	0.000	4.2
$S_3(n\pi^*)$	3.60	0.000	2.6
$S_4(\pi\pi^*)$	4.29	0.026	4.1
$S_5(\pi\pi^*)$	4.38	0.020	0.9
$S_6(n\pi^*)$	4.70	0.000	6.8

Table S2: Emission properties of 1-HAQ. Adiabatic energy, (E^a in *eV*, bold), fluorescence energy, *(E_{fl},* given in parenthesis), excited-state dipole moment (μ_e in *D*) and oscillator strength (*f*) of the given excited-state form optimized with the CC2/cc-pVDZ method.

1-HAQ				
state/ tautomer	***$E^a(S_n)$*** (E_{fl})	μ_e /*D*	*f*	
form K(I)				
S_0	**0.00**			
S_1 $^{\pi\pi*}$	-	-	-	
S_1 $^{n\pi^*}$	**2.75** (2.18)	μ_e = 4.2 D	**0.00**	
form E(II)				
S_0	-			
S_1 $^{\pi\pi*}$	**2.67** (1.92)	μ_e = 1.2 D	**0.200**	
S_1 $^{n\pi^*}$	**2.60** (1.38)	μ_e = 5.4 D	**0.000**	

Table S3: Emission properties of 1,4-HAQ. Adiabatic energy, (E^a in *eV*, bold), fluorescence energy, *(E_{fl},* given in parenthesis), excited-state dipole moment (μ_e in *D*) and oscillator strength (*f*) of the given excited-state form optimized with the CC2/cc-pVDZ method.

1,4-HAQ				
state/ tautomer	***S_n*** (E_{fl})	μ_e /*D*	*f*	
form KK(I)				
S_0	***0.00***			
S_1 (ππ*)	**2.39** (2.13)	0.1 D	0.221	
S_1(nπ*)	**2.95** (2.42)	3.1 D	**0.000**	
form EE(II)				
S_0	***0.36***			
S_1 (ππ*)	**2.50** (2.01)	2.6 D	**0.225**	
S_1(nπ*)	**3.10** (2.57)	2.0 D	**0.000**	
form EK ~ KE				
S_0	-			
S_1 (ππ*)	-	-	-	
S_1(nπ*)	**2.66** (1.70)	3.6 D	**0.000**	